Analysis of SARS-CoV-2 Antibodies in COVID-19 Convalescent Plasma using a Coronavirus Antigen Microarray

Authors

Rafael R. de Assis (1)
Aarti Jain (1)
Rie Nakajima (1)
Algis Jasinskas (1)
Jiin Felgner (1)
Joshua M. Obiero (1)
Oluwasanmi Adenaiye (2)
Sheldon Tai (2)
Filbert Hong (2)
Philip Norris (3)
Mars Stone (3)
Graham Simmons (3)
Anil Bagri (4)
Martin Schreiber (5)
Andreas Buser (6)
Andreas Holbro (6)
Manuel Battegay (6)
Donald K. Milton (2)
Prometheus Study Group
Huw Davies (1)
Laurence M. Corash (4)
Michael P. Busch (3)
Philip L. Felgner (1)
Saahir Khan (8)*
*Corresponding Author: saahirk@uci.edu

Affiliations

1. Department of Physiology and Biophysics, School of Medicine, University of California Irvine, Irvine, CA
2. Institute for Applied Environmental Health, School of Public Health, University of Maryland, College Park, MD
3. Vitalant Research Institute, San Francisco, CA
4. Cerus Corporation, Concord, CA
5. Department of Surgery, Oregon Health & Science University, Portland, OR
6. Regional Blood Transfusion Service, Swiss Red Cross, University Hospital Basel, University of Basel, Basel, Switzerland
7. Division of Infectious Diseases & Hospital Epidemiology, University Hospital Basel, University of Basel, Basel, Switzerland
8. Division of Infectious Diseases, Department of Medicine, University of California Irvine Health, Orange, CA

Abstract

The current practice for diagnosis of COVID-19, based on SARS-CoV-2 PCR testing of pharyngeal or respiratory specimens in a symptomatic patient at high epidemiologic risk, likely underestimates the true prevalence of infection. Serologic methods can more accurately estimate the disease burden by detecting infections missed by the limited testing performed to date. Here, we describe the validation of a coronavirus antigen microarray containing immunologically significant antigens from SARS-CoV-2, in addition to SARS-CoV, MERS-CoV, common human coronavirus strains, and other common respiratory viruses. A comparison of antibody profiles detected on the array from control sera collected prior to the SARS-CoV-2 pandemic versus convalescent blood specimens from virologically confirmed COVID-19 cases demonstrates complete discrimination of these two groups. This array can be used as a diagnostic tool, as an epidemiologic tool to more accurately estimate the disease burden of COVID-19, and as a research tool to correlate antibody responses with clinical outcomes.

Background

COVID-19 caused by the SARS-CoV-2 virus is a worldwide pandemic with significant morbidity and mortality estimates from 1-4% of confirmed cases[1]. The current case definition for confirmed SARS-CoV-2 infection relies on PCR-positive pharyngeal or respiratory specimens, with testing largely determined by presence of fever or respiratory symptoms in an individual at high epidemiologic risk. However, this case definition likely underestimates true prevalence, as individuals who develop subclinical infection that does not produce fever or respiratory symptoms are unlikely to be tested, and testing by PCR of pharyngeal or respiratory specimens is only around 60-80% sensitive depending on sampling location and technique and the patient's viral load[2]. Widespread testing within the United States is also severely limited by the lack of available testing kits and testing capacity limitations of available public and private laboratories. Therefore, the true prevalence of SARS-CoV-2 infection is likely much higher than currently reported case numbers would indicate.

Serology can play an important role in defining the true prevalence of COVID-19, particularly for subclinical infection[2]. Early studies of serology demonstrate high sensitivity to detect confirmed SARS-CoV-2 infection, with antibodies to virus detected approximately 1 to 2 weeks after symptom onset[3]. Unlike PCR positivity, SARS-CoV-2 antibodies are detectable throughout the disease course and persist indefinitely[4]. Multiple serologic tests have been developed for COVID-19[5] including a recently FDA-approved lateral flow assay. However, these tests are limited to detection of antibodies against one or two antigens, and cross-reactivity with antibodies to other human coronaviruses that are present in all adults[6] is currently unknown. Prior use of serology for detection of emerging coronaviruses focused on antibodies against the spike (S) protein, particularly the S1 domain, and the nucleocapsid (N) protein[7]. However, the optimal set of antigens to detect strain-specific coronavirus antibodies remains unknown.

Protein microarray technology can be used to detect antibodies of multiple isotypes against hundreds of antigens in a high throughput manner[8,9] so is well suited to serologic surveillance studies. This technology, which has previously been applied to other emerging coronaviruses[10], is based on detection of binding antibodies, which are well-correlated with neutralizing antibodies[11] but do not require viral culture in biosafety level 3 facilities. Recently, our group developed a coronavirus antigen microarray (CoVAM) that includes antigens from SARS-CoV-2 and tested it on human sera collected prior to the pandemic to demonstrate low cross-reactivity with antibodies from human coronaviruses that cause the common cold, particularly for the S1 domain[2]. Here, we further validate this methodology using convalescent blood specimens from COVID-19 cases confirmed by positive SARS-CoV-2 PCR.

Methodology

Specimen Collection

The SARS-CoV-2 convalescent blood specimens from nasopharyngeal SARS-CoV-2 PCR-positive individuals were collected from different sources to increase the number of positive specimens available for analysis. Two sera and plasma samples were obtained from acute COVID-19 patients from the Oregon Health Sciences University Hospital

(OHSU), Portland, OR. These were sourced from discarded clinical laboratory specimens exempted from informed consent and IRB approval under condition of patient anonymity. Four plasma samples were obtained from outpatients of the University Hospital Basel, University of Basel, Basel, Switzerland. These patients were screened in accordance with Swiss regulations on blood donation and approved as plasma donors according to the Blood Transfusion Service of the Swiss Red Cross with informed consent. These donors were diagnosed with COVID-19 based on SARS-CoV-2 positive nasopharyngeal swab PCR tests. At time of plasma donation, each had two negative nasopharyngeal swab SARS-CoV-2 PCR- tests and negative SARS-CoV-2 PCR tests in blood, and they were qualified as plasma donors. Plasma was collected from these convalescent donors at the Regional Blood Transfusion Service of the Swiss Red Cross in accordance with national regulations. One convalescent plasma was isolated from a large-volume apheresis collection following standard protocol from a documented recovered COVID-19 blood donor who was more than 28 days post symptomatic.

The negative control sera used in this study were collected between November 2018 and May 2019 for a larger study where residents of a college resident community in the Eastern United States were monitored prospectively to identify acute respiratory infection (ARI) cases using questionnaires and RT-qPCR, so as to characterize contagious phenotypes including social connections, built environment, and immunologic phenotypes[12]. A total of 144 de-identified blood specimens were tested on the CoV antigen microarray. Electronic informed consents including future research use authorization was obtained under protocols approved by the Institutional Review Boards (IRBs) of the University of Maryland and the Department of Navy Human Research Protections Office.

Coronavirus Antigen Microarray

The coronavirus antigen microarray used in this investigation includes 67 antigens across subtypes expressed in either baculovirus or HEK-293 cells (Table 1). These antigens were provided by Sino Inc. (Wayne, PA) as either catalog products or custome synthesis service products. The antigens were printed onto microarrays, probed with human sera, and analyzed as previously described[9,13,14].

Briefly, lyophilized antigens were reconstituted to a concentration of 0.1 mg/mL in phosphate-buffered saline (PBS) with 0.001% Tween-20 (T-PBS) and then printed onto nitrocellulose-coated slides from Grace Bio Labs (GBL, Bend, OR) using an OmniGrid 100 microarray printer (GeneMachines). The microarray slides were probed with human sera diluted 1:100 in 1x GVS Fast Blocking Buffer (Fischer Scientific) overnight at 4°C, washed with T-TBS buffer (20 mM Tris-HCl, 150 mM NaCl, 0.05% Tween-20 in ddH_2O adjusted to pH 7.5 and filtered) 3 times for 5 minutes each, labeled with secondary antibodies to human IgA and IgG conjugated to quantum dot fluorophores for 2 hours at room temperature, and then washed with T-TBS 3 times for 5 minutes each and dried. The slides were imaged using ArrayCam imager (Grace Bio Labs, Bend, OR) to measure background-subtracted median spot fluorescence. Non-specific binding of secondary antibodies was subtracted using saline control. Mean fluorescence of the 4 replicate spots for each antigen was used for analysis.

Statistical Analyses

The mean fluorescence intensity (MFI) of each antigen was determined by the average of the median fluorescence signal of four replicate spots. The fluorescence signal for each spot was determined by its signal intensity subtracted by the background fluorescence. Antigens containing a human Fc tag were removed from the analysis, as the secondary antibodies used for quantification are known to bind to human Fc; non-human Fc tag did not interfere with the assay. All statistical analyses were conducted using R version 3.6.3 (R Foundation for Statistical Computing, Vienna, Austria).
MFI was normalized using the *normalize.quantiles.use.target* function from the *proprocessCore* package (version 1.48.0). As a target for normalization, a vector containing the median MFI for IgG or IgA was constructed. Descriptive statistics were used to summarize the IgA and IgG reactivity measured as MFI. Wilcoxon Rank Sum tests with $p < 0.05$ corrected for multiple comparisons were used to compare the mean differences between groups.
Receiver Operating Characteristic Area Under the Curve (ROC AUC) values for each antigen were calculated by comparing positive and negative specimens using the *pROC* package (version 1.16.2). Antigens were ranked based on their ROC AUC values, and high performing antigens with ROC AUC $\geq$ 0.95 were identified. Data visualization was performed using the *ggplot2* package (version 3.3.0).

Results

Discrimination of SARS-CoV-2 Convalescent Plasma using Coronavirus Antigen Microarray

The coronavirus antigen microarray was used to detect IgG and IgA antibodies against a panel of antigens, including coronavirus spike protein (S) as separated receptor-binding (RBD), S1, and S2 domains or whole protein (S1+S2) and nucleocapsid protein (NP), from multiple coronaviruses including SARS-CoV-2, SARS-CoV, MERS-CoV, and the four common cold coronaviruses (HKU1, OC43, NL63, 229E) as listed in Table 1.
To determine the antibody profile of SARS-CoV-2 infection, the differential reactivity to these antigens was evaluated for SARS-CoV-2 convalescent plasma from PCR-positive individuals (positive group) and sera collected prior to the COVID-19 pandemic from naïve individuals (negative group) as shown in Figure 1.
The positive group demonstrates high IgG reactivity to SARS-CoV-2 NP, S2, and S1+S2 antigens and moderate IgG reactivity to SARS-CoV-2 S1 and RBD antigens, while the negative group demonstrates low IgG cross-reactivity to SARS-CoV-2 S1+S2 and no cross-reactivity to other SARS-CoV-2 antigens (Figure 2). The positive group also demonstrates high IgG cross-reactivity with SARS-CoV NP and MERS-CoV S2 and S1+S2 antigens, while the negative group demonstrates low cross-reactivity with MERS-CoV S1+S2 and no cross-reactivity with other SARS-CoV and MERS-CoV antigens. The two groups do not differ significantly in reactivity to common cold coronaviruses and other seasonally circulating respiratory viruses.
Similar trends are observed for IgA but with lower reactivity overall (Figure 3). The positive group again demonstrates high IgA reactivity to SARS-CoV-2 NP, S2, and

S1+S2 and moderate IgA reactivity to SARS-CoV-2 S1 with high IgA cross-reactivity to SARS-CoV NP, while the negative group demonstrates low IgA cross-reactivity to all SARS-CoV-2, SARS-CoV, and MERS-CoV antigens.

Selection of High-Performing Antigens to Detect SARS-CoV-2 Infection

Each coronavirus antigen was evaluated for performance in discriminating the positive group from the negative group across a full range of assay cutoff values to generate Receiver Operating Characteristic (ROC) curves for which Area Under Curve (ROC AUC) was measured (Figure 4). High-performing antigens for detection of IgG or IgA defined by ROC AUC $\geq$ 0.95 included all SARS-CoV-2 antigens and MERS-CoV S2 for IgG and SARS-CoV-2 S2 and S1+S2 for IgA (Table 2). Each of these antigens discriminated between the positive group and the negative group with high significance (Figure 5).

Discussion

This study reveals several insights into the antibody response to SARS-CoV-2 infection. The antibody profiles of naïve individuals include high IgG reactivity to common cold coronaviruses with low-level cross-reactivity with S2 domains from SARS-CoV-2 and other epidemic coronaviruses, which is not surprising given the high degree of sequence homology and previously observed serologic cross-reactivity[15] between S2 domains of betacoronaviruses, a group that includes SARS-CoV-2, SARS-CoV, MERS, and common cold coronaviruses HKU1 and OC43. However, naïve individuals do not show cross-reactivity to other SARS-CoV-2 antigens. Even for the nucleocapsid protein, which also has high sequence homology between betacoronaviruses, cross-reactivity is only seen between SARS-CoV-2 and SARS-CoV and not with MERS-CoV or common cold coronaviruses. In addition, the quantitative difference between high antibody reactivity to SARS-CoV-2 S2 in the positive group and low-level antibody cross-reactivity in the negative group is large enough that these antigens still discriminate these groups with high significance.

This study also informs antigen selection and design for population surveillance and clinical diagnostic assays and vaccine development. The observation that naïve individuals with antibodies to common cold coronaviruses do not show cross-reactivity to SARS-CoV-2 nucleocapsid protein dispels concerns that the high sequence homology of this protein across betacoronaviruses would impair its performance as a diagnostic or vaccine antigen. The low-level antibody cross-reactivity of naïve individuals for SARS-CoV-2 spike protein containing S2 domain may not preclude its use as a diagnostic antigen given large quantitative difference in antibody reactivity between positive and negative groups, but this cross-reactivity may influence response to vaccination with spike protein antigens containing the S2 domain.

The coronavirus antigen microarray can be useful both as an epidemiologic tool and as a research tool. The high throughput detection of SARS-CoV-2-specific antibody profiles that reliably distinguish COVID-19 cases from negative controls can be applied to large-scale population surveillance studies for a more accurate estimation of the true prevalence of disease than can be achieved with symptom-based PCR testing. In

addition, detection of these antibodies in SARS-CoV-2 convalescent plasma donations can provide validation prior to clinical use for passive immunization. The variation in the SARS-CoV-2 antibody profiles among acute and convalescent donors suggests that epitope characterization of convalescent donor plasma will be informative for evaluation of passive immune therapy efficacy in COVID-19 patients. The central role of inflammation in the pathogenesis of severe COVID-19[16] can be more closely studied by analyzing both strain-specific and cross-reactive antibody responses, particularly to test hypotheses regarding antibody-dependent enhancement with critical implications for vaccine development[17].

Conclusions

A coronavirus antigen microarray containing a panel of antigens from SARS-CoV-2 in addition to other human coronaviruses was able to reliably distinguish convalescent plasma of PCR-positive COVID-19 cases from negative control sera collected prior to the pandemic by detecting both strain-specific and cross-reactive antibodies. Further studies are needed to apply this methodology to large-scale serologic surveillance studies and to correlate specific antibody responses with clinical outcomes.

Acknowledgements

Saahir Khan is supported by the National Center for Research Resources and the National Center for Advancing Translational Sciences, National Institutes of Health, through Grant KL2 TR001416. The content is solely the responsibility of the authors and does not necessarily represent the official views of the NIH.
Prometheus-UMD was sponsored by the Defense Advanced Research Projects Agency (DARPA) BTO under the auspices of Col. Matthew Hepburn through agreements N66001-17-2-4023 and N66001-18-2-4015 (PI: Milton). This study was funded in part by the Defense Threat Reduction Agency via grants HDTRA1-18-1-0036 (PI: Davies) and HDTRA1-18-1-0035 (PI: Felgner). The findings and conclusions in this report are those of the authors and do not necessarily represent the official position or policy of the funding agencies and no official endorsements should be inferred.

Author Disclosures

The coronavirus antigen microarray is intellectual property of the Regents of the University of California that is licensed for commercialization to Nanommune Inc. (Irvine, CA), a private company for which Philip L. Felgner is the largest shareholder and several co-authors (de Assis, Jain, Nakajima, Jasinskas, Obiero, Davies, and Khan) also own shares. Nanommune Inc. has a business partnership with Sino Biological Inc. (Beijing, China) which expressed and purified the antigens used in this study.
The convalescent plasma used in this study was collected for clinical use by independent blood centers using licensed plasma or platelet processing systems manufactured by Cerus Corporation, for which multiple authors (Corash, Bagri) are shareholders and employees. Manuel Battegay, Andreas Buser and Andreas Holbro are employees of the University of Basel and have no conflicts of interest.

References

1 Cao, Y., Liu, X., Xiong, L. & Cai, K. Imaging and Clinical Features of Patients With 2019 Novel Coronavirus SARS-CoV-2: A systematic review and meta-analysis. *J Med Virol*, doi:10.1002/jmv.25822 (2020).

2 Tang, Y. W., Schmitz, J. E., Persing, D. H. & Stratton, C. W. The Laboratory Diagnosis of COVID-19 Infection: Current Issues and Challenges. *J Clin Microbiol*, doi:10.1128/JCM.00512-20 (2020).

3 Zhao, J. *et al.* Antibody responses to SARS-CoV-2 in patients of novel coronavirus disease 2019. *Clin Infect Dis*, doi:10.1093/cid/ciaa344 (2020).

4 To, K. K. *et al.* Temporal profiles of viral load in posterior oropharyngeal saliva samples and serum antibody responses during infection by SARS-CoV-2: an observational cohort study. *Lancet Infect Dis*, doi:10.1016/S1473-3099(20)30196-1 (2020).

5 Liu, W. *et al.* Evaluation of Nucleocapsid and Spike Protein-based ELISAs for detecting antibodies against SARS-CoV-2. *J Clin Microbiol*, doi:10.1128/JCM.00461-20 (2020).

6 Zhou, W., Wang, W., Wang, H., Lu, R. & Tan, W. First infection by all four non-severe acute respiratory syndrome human coronaviruses takes place during childhood. *BMC Infect Dis* **13**, 433, doi:10.1186/1471-2334-13-433 (2013).

7 Agnihothram, S. *et al.* Evaluation of serologic and antigenic relationships between middle eastern respiratory syndrome coronavirus and other coronaviruses to develop vaccine platforms for the rapid response to emerging coronaviruses. *J Infect Dis* **209**, 995-1006, doi:10.1093/infdis/jit609 (2014).

8 Davies, D. H. *et al.* Profiling the humoral immune response to infection by using proteome microarrays: high-throughput vaccine and diagnostic antigen discovery. *Proc Natl Acad Sci U S A* **102**, 547-552, doi:10.1073/pnas.0408782102 (2005).

9 Khan, S. *et al.* Use of an Influenza Antigen Microarray to Measure the Breadth of Serum Antibodies Across Virus Subtypes. *J Vis Exp*, doi:10.3791/59973 (2019).

10 Reusken, C. *et al.* Specific serology for emerging human coronaviruses by protein microarray. *Euro Surveill* **18**, 20441, doi:10.2807/1560-7917.es2013.18.14.20441 (2013).

11 Chan, C. M. *et al.* Examination of seroprevalence of coronavirus HKU1 infection with S protein-based ELISA and neutralization assay against viral spike pseudotyped virus. *J Clin Virol* **45**, 54-60, doi:10.1016/j.jcv.2009.02.011 (2009).

12 Zhu, S. *et al.* Ventilation and laboratory confirmed acute respiratory infection (ARI) rates in college residence halls in College Park, Maryland. *Environ Int* **137**, 105537, doi:10.1016/j.envint.2020.105537 (2020).

13 Jain, A. *et al.* Evaluation of quantum dot immunofluorescence and a digital CMOS imaging system as an alternative to conventional organic fluorescence dyes and laser scanning for quantifying protein microarrays. *Proteomics* **16**, 1271-1279, doi:10.1002/pmic.201500375 (2016).

14 Nakajima, R. *et al.* Protein Microarray Analysis of the Specificity and Cross-Reactivity of Influenza Virus Hemagglutinin-Specific Antibodies. *mSphere* **3**, doi:10.1128/mSphere.00592-18 (2018).

15 Patrick, D. M. *et al.* An Outbreak of Human Coronavirus OC43 Infection and Serological Cross-reactivity with SARS Coronavirus. *Can J Infect Dis Med Microbiol* **17**, 330-336, doi:10.1155/2006/152612 (2006).

16 Shi, Y. *et al.* COVID-19 infection: the perspectives on immune responses. *Cell Death Differ*, doi:10.1038/s41418-020-0530-3 (2020).

17 Peeples, L. News Feature: Avoiding pitfalls in the pursuit of a COVID-19 vaccine. *Proceedings of the National Academy of Sciences*, 202005456, doi:10.1073/pnas.2005456117 (2020).

Figures and Tables

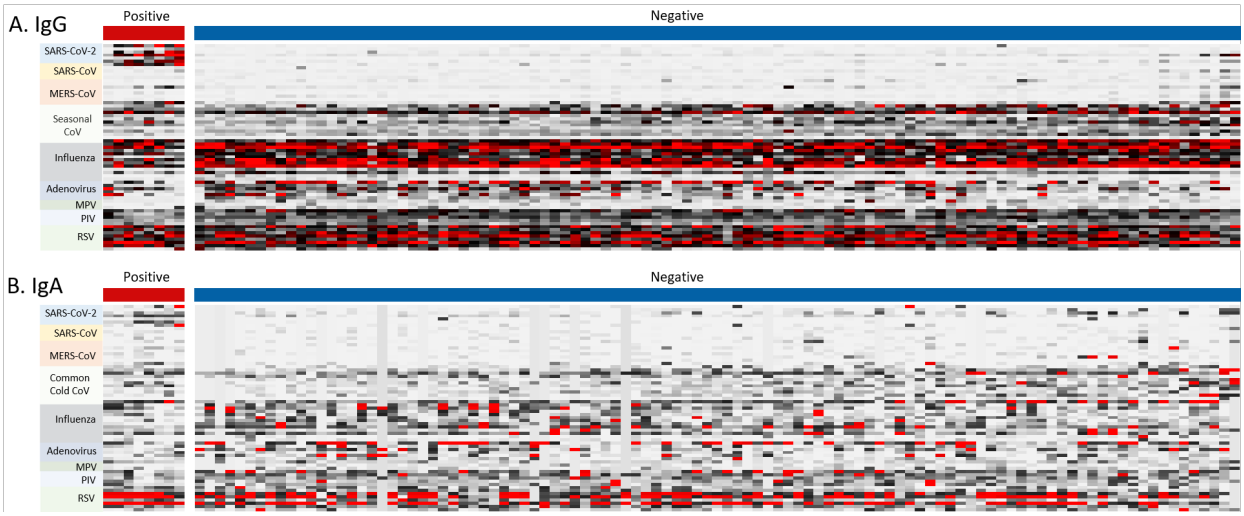

Figure 1. Heatmap for coronavirus antigen microarray. The heatmap shows IgG (A) and IgA (B) reactivity measured as mean fluorescence intensity across four replicates, against each antigen organized into rows color coded by virus, for sera organized into columns classified as positive (convalescent from PCR-positive individuals) or negative (prior to pandemic from naïve individuals). Reactivity is represented by color (white = low, black = mid, red = high).

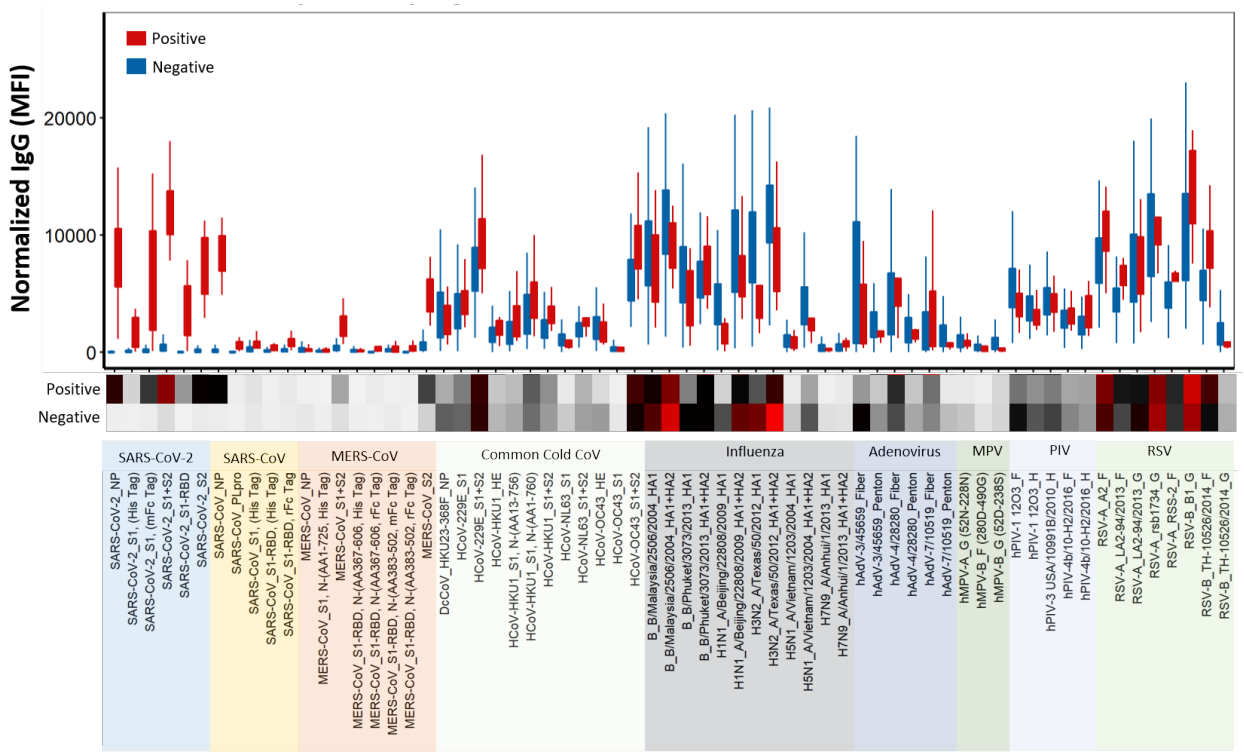

Figure 2. Normalized IgG reactivity of positive and negative sera on coronavirus antigen microarray. The plot show IgG reactivity against each antigen measured as mean fluorescence intensity (MFI) with full range (bars) and interquartile range (boxes) for convalescent sera from PCR-positive individuals (positive, red) and sera from naïve individuals prior to pandemic (negative, blue). Below the plot, the heatmap shows average reactivity for each group (white = low, black = mid, red = high). The antigen labels are color coded for respiratory virus group.

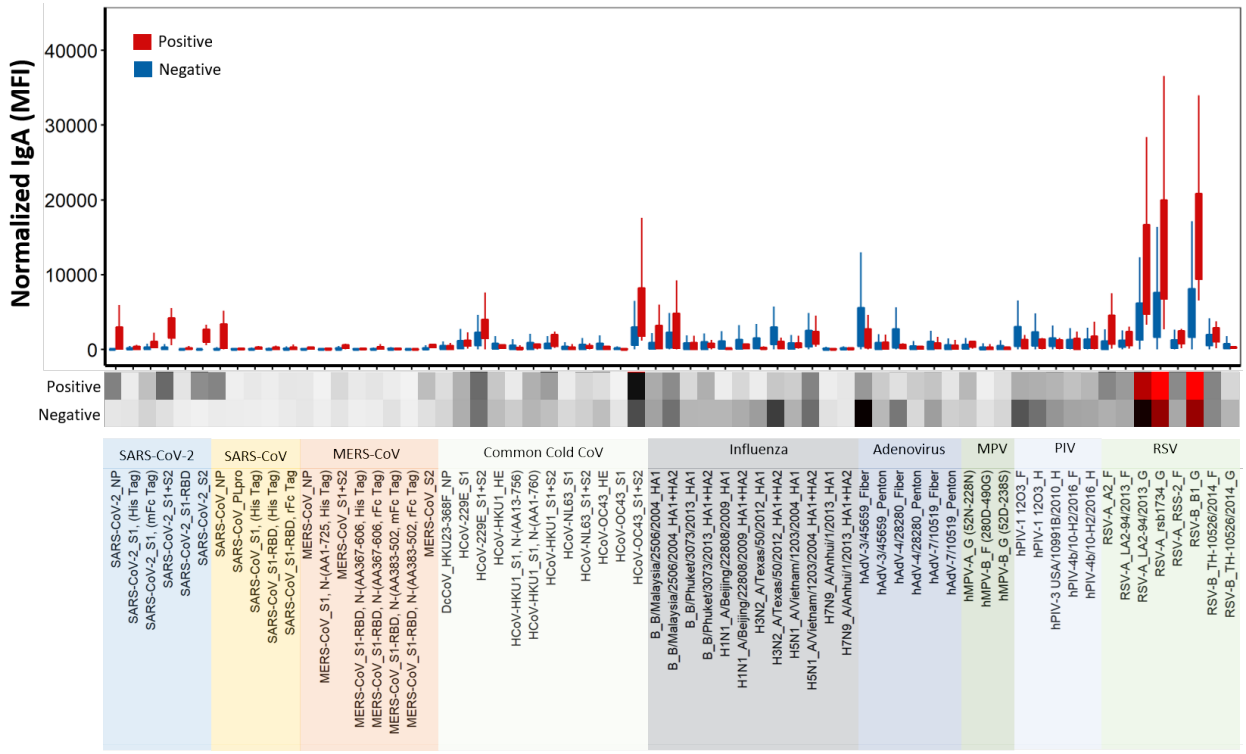

Figure 3. Normalized IgA reactivity of positive and negative sera on coronavirus antigen microarray. The plot show IgG reactivity against each antigen measured as mean fluorescence intensity (MFI) with full range (bars) and interquartile range (boxes) for convalescent sera from PCR-positive individuals (positive, red) and sera from naïve individuals prior to pandemic (negative, blue). Below the plot, the heatmap shows average reactivity for each group (white = low, black = mid, red = high). The antigen labels are color coded for respiratory virus group.

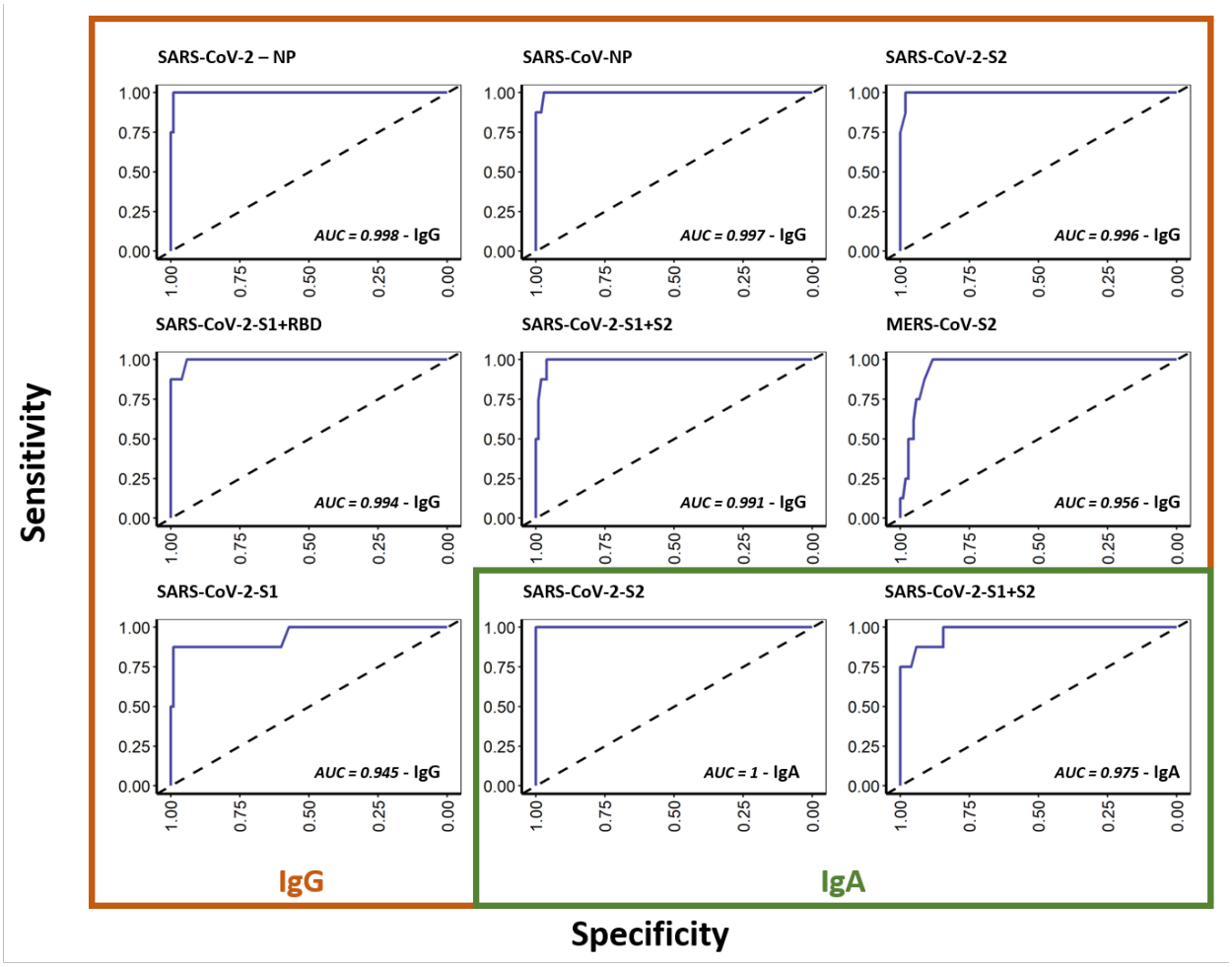

Figure 4. ROC curves for high-performing antigens. ROC curves showing sensitivity versus specificity for discrimination of positive and negative sera were derived for each individual high performing antigen (ROC AUC $\geq$ 0.95) for both IgG and IgA (solid blue line) and compared to no discrimination (ROC AUC = 0.5, dashed black line).

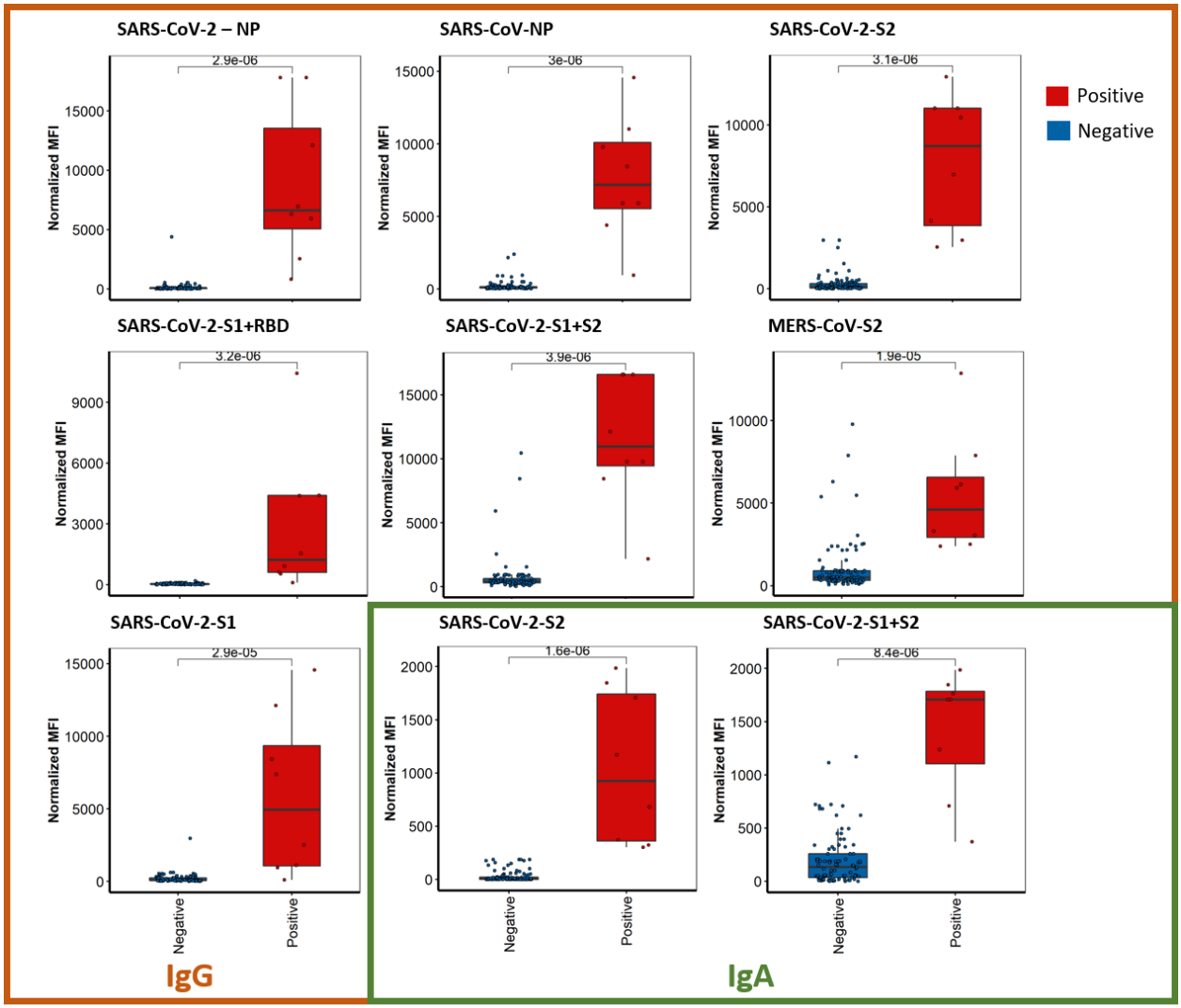

Figure 5. Normalized antibody reactivity of positive and negative sera for high-performing antigens. IgG and IgA reactivity against each high-performing antigens (ROC AUC $\geq$ 0.95) measured as mean fluorescence intensity (MFI) for convalescent sera from PCR-positive individuals (positive, red) and sera from naïve individuals prior to pandemic (negative, blue) are shown as box plots, including full range (bars), interquartile range (boxes), median (black line), and individual sera (dots) with p-values for each antigen calculated by Wilcoxon Rank Sum test.

Virus	Subtype	Strain	Protein	GenBank	Expression	Construct	Source	Cat. No.
CoV	Beta	SARS-CoV-2	NP		Baculovirus	N-(AA)-His-C	Sino	40588-V08B
CoV	Beta	SARS-CoV-2	S1-RBD		HEK293	N-(AA)-mFc-C	Sino	40592-V05H
CoV	Beta	SARS-CoV-2	S1		HEK293	N-(AA)-His-C	Sino	40591-V08H
CoV	Beta	SARS-CoV-2	S1		HEK293	N-(AA)-mFc-C	Sino	40591-V02H
CoV	Beta	SARS-CoV-2	S1		HEK293	N-(AA)-Fc-C	Sino	40591-V05H1
CoV	Beta	SARS-CoV-2	S2		Baculovirus	N-(AA)-His-C	Sino	40590-V08B
CoV	Beta	SARS-CoV-2	S1+S2		Baculovirus	N-(AA)-His-C	Sino	40589-V08B1
CoV	Beta	SARS	PLpro	AAX16193.1	E. coli	N-(AA1541-1859)-His-C	Sino	40524-V08E
CoV	Beta	SARS	S1-RBD	AAX16192.1	Baculovirus	N-(AA306-527)-Fc-C	Sino	40150-V31B2
CoV	Beta	SARS	S1-RBD	AAX16192.1	Baculovirus	N-(AA306-527)-His-C	Sino	40150-V08B2
CoV	Beta	SARS	S1	AAX16192.1	Baculovirus	N-(AA1-667)-His-C	Sino	40150-V08B1
CoV	Beta	SARS	NP	NP_828858.1	Baculovirus	N-(AA1-422)-His-C	Sino	40143-V08B
CoV	Beta	MERS	NP	AFS88943.1	Baculovirus	N-(AA1-413)-His-C	Sino	40068-V08B
CoV	Beta	MERS	S1-RBD	AFS88936.1	Baculovirus	N-(AA383-502)-Fc-C	Sino	40071-V05B
CoV	Beta	MERS	S1-RBD	AFS88936.1	Baculovirus	N-(AA383-502)-rFc-C	Sino	40071-V31B
CoV	Beta	MERS	S1-RBD	AFS88936.1	Baculovirus	N-(AA367-606)-rFc-C	Sino	40071-V31B1
CoV	Beta	MERS	S1-RBD	AFS88936.1	Baculovirus	N-(AA367-606)-His-C	Sino	40071-V08B1
CoV	Beta	MERS	S1	AFS88936.1	HEK293	N-(AA1-725)-His-C	Sino	40069-V08H
CoV	Beta	MERS	S1	AFS88936.1	Baculovirus	N-(AA1-725)-His-C	Sino	40069-V08B1
CoV	Beta	MERS	S1+S2	AFS88936.1	Baculovirus	N-(AA1-1297)-His-C	Sino	40069-V08B
CoV	Beta	MERS	S2	AFS88936.1	Baculovirus	N-(AA726-1296)-His-C	Sino	40070-V08B
CoV	Alpha	NL63	S1	A0A1L2YVI8	HEK293	N-(AA19-717)-His-C	Sino	40600-V08H
CoV	Alpha	NL63	S1+S2	A0A1L2YVI8	Baculovirus	N-(AA19-1296)-His-C	Sino	40604-V08B
CoV	Alpha	229E	S1	A0A1L7B942	HEK293	N-(AA16-536)-His-C	Sino	40601-v08H
CoV	Alpha	229E	S1+S2	A0A1L7B942	Baculovirus	N-(AA16-1115)-His-C	Sino	40605-V08B
CoV	Beta	HKU1	S1	YP_173238.1	HEK293	N-(AA1-760)-His-C	Sino	40021-V08H
CoV	Beta	HKU1	S1	Q0ZME7	HEK293	N-(AA13-756)-His-C	Sino	40602-V08H
CoV	Beta	HKU1	S1+S2	Q0ZME7	Baculovirus	N-(AA13-1295)-His-C	Sino	40606-V08B
CoV	Beta	HKU1	HE	Q0ZME7	HEK293	N-(AA16-394)-His-C	Sino	Custom
CoV	Beta	HKU23-368F	NP	AHN64796.1	HEK293	N-(AA1-448)-His-C	Sino	40458-V08B
CoV	Beta	OC43	S1	AVR40344.1	HEK293	N-(AA13-533)-His-C	Sino	Custom
CoV	Beta	OC43	S1+S2	AVR40344.1	Baculovirus	N-(AA13-1304)-His-C	Sino	40607-V08B
CoV	Beta	OC43	HE	ATN39879.2	HEK293	N-(AA16-394)-His-C	Sino	40603-V08H
RSV	A	LA2-94/2013	F	A0A023RA53	Baculovirus	N-(AA1-526)-His-C	Sino	Custom
RSV	A	LA2-94/2013	G	A0A076FRQ0	HEK293	N-(AA64-321)-His-C	Sino	Custom
RSV	A	A2	F		Baculovirus	N-(AA1-529)-His-C	Sino	11049-V08B
RSV	A	rsb1734	G		HEK293	N-(AA66-297)-His-C	Sino	11070-V08H
RSV	A	RSS-2	F		Baculovirus	N-(AA1-529)-His-C	Sino	40037-V08B
RSV	B	TH-10526/2014	F	K7WLI9	Baculovirus	N-(AA1-525)-His-C	Sino	Custom
RSV	B	TH-10526/2014	G	A0A142MLK4	HEK293	N-(AA64-310)-His-C	Sino	Custom
RSV	B	B1	G		HEK293	N-(AA67-299)-His-C	Sino	13029-V08H
MPV	A	PER/CFI0320/2010/A	G		HEK293	52N-228N-His	Sino	Custom
MPV	B	PER/CFI0466/2010/B	G		HEK293	52D-238S-His	Sino	Custom
MPV	B	PER/CFI0320/2010/A	F		HEK293	280D-490G-His	Sino	Custom
PIV	1	12O3	F	A0A1V0E1X5	Baculovirus	N-(AA22-497)-His-C	Sino	Custom
PIV	1	12O3	H	A0A1B2CW87	Baculovirus	N-His-(AA60-575)-C	Sino	Custom
PIV	3	USA/10991B/2010	H	T1UD13	Baculovirus	N-His-(AA55-575)-C	Sino	Custom
PIV	4	hPIV-4b/10-H2/2016	F	A0A1V0E1N6	Baculovirus	N-(AA22-486)-His-C	Sino	Custom
PIV	4	hPIV-4b/10-H2/2016	H	A0A1V0E1N4	Baculovirus	N-His-(AA48-575)-C	Sino	Custom
Adeno	3	hAdV-3/45659	Fiber	P04501	E. coli	N-His-[Prot]-C	Sino	Custom
Adeno	3	hAdV-3/45659	Penton	Q2Y0H9	Baculovirus	N-His-[Prot]-C	Sino	Custom
Adeno	4	hAdV-4/28280	Fiber	P36844	Baculovirus	N-[Prot]-His-C	Sino	Custom
Adeno	4	hAdV-4/28280	Penton	Q2KSF3	Baculovirus	N-[Prot]-His-C	Sino	Custom
Adeno	7	Adeno7 10519	Fiber	P15141	Baculovirus	N-His-[Prot]-C	Sino	Custom
Adeno	7	Adeno7 10519	Penton	Q2KS58	Baculovirus	N-[Prot]-His-C	Sino	Custom
Flu	H1N1	A/Beijing/22808/2009	HA1	ADD64203.1	HEK293	N-(AA1-344)-His-C	Sino	40035-V08H1
Flu	H1N1	A/Beijing/22808/2009	HA1+HA2	ADD64203.1	HEK293	N-(AA1-529)-His-C	Sino	40035-V08H
Flu	H3N2	A/Texas/50/2012	HA1	AGL07159.1	HEK293	N-(AA1-345)-His-C	Sino	40354-V08H1
Flu	H3N2	A/Texas/50/2012	HA1+HA2	AGL07159.1	Baculovirus	N-(AA1-530)-His-C	Sino	40354-V08B
Flu	B	B/Malaysia/2506/2004	HA1	CO05957.1	HEK293	N-(AA1-362)-His-C	Sino	11716-V08H1
Flu	B	B/Malaysia/2506/2004	HA1+HA2	CO05957.1	HEK293	N-(AA1-556)-His-C	Sino	11716-V08H
Flu	B	B/Phuket/3073/2013	HA1	EPI529345	HEK293	N-(AA1-361)-His-C	Sino	40498-V08H1
Flu	B	B/Phuket/3073/2013	HA1+HA2	EPI529345	Baculovirus	N-(AA1-547)-His-C	Sino	40498-V08B
Flu	H5N1	A/Vietnam/1203/2004	HA1	AAW80717.1	HEK293	(AA1-342)-mFcg1-His	Sino	10003-V06H1
Flu	H5N1	A/Vietnam/1203/2004	HA1+HA2	AAW80717.1	HEK293	(AA1-531)-mFcg1-His	Sino	10003-V06H3
Flu	H7N9	A/Anhui/1/2013	HA1	AGJ51953.1	HEK293	N-(AA1-338)-His-C	Sino	40103-V08H1
Flu	H7N9	A/Anhui/1/2013	HA1+HA2	AGJ51953.1	HEK293	N-(AA1-524)-His-C	Sino	40103-V08H

Table 1. Content of coronavirus antigen microarray. The virus group, subtype, and strain, protein, GenBank identification where available, expression system, gene construct, and vendor source and catalog number are shown for each antigen.

IgG Rank	Epitope	AUC	IgA Rank	Antigen	AUC
1	SARS-CoV-2_NP	0.998	1	SARS-CoV-2_S2	1
2	SARS-CoV_NP	0.997	2	SARS-CoV-2_S1+S2	0.975
3	SARS-CoV-2_S2	0.996	3	MERS-CoV_S1+S2	0.791
4	SARS-CoV-2_S1-RBD	0.994	4	SARS-CoV-2_NP	0.753
5	SARS-CoV-2_S1+S2	0.991	5	MERS-CoV_S2	0.752
6	MERS-CoV_S2	0.956	6	MERS-CoV_S1-RBD, N-(AA383-502, rFc Tag)	0.751
7	SARS-CoV-2_S1, (mFc Tag)	0.945	7	SARS-CoV-2_S1-RBD	0.735
8	MERS-CoV_S1-RBD, N-(AA367-606, His Tag)	0.894	8	MERS-CoV_S1, N-(AA1-725, His Tag)	0.734
9	MERS-CoV_S1, N-(AA1-725, His Tag)	0.845	9	SARS-CoV-2_S1, (mFc Tag)	0.72
10	MERS-CoV_S1+S2	0.836	10	SARS-CoV_NP	0.714
11	MERS-CoV_NP	0.829	11	SARS-CoV_S1-RBD, rFc Tag	0.684
12	SARS-CoV_S1-RBD, rFc Tag	0.763	12	MERS-CoV_S1-RBD, N-(AA367-606, rFc Tag)	0.65
13	MERS-CoV_S1-RBD, N-(AA383-502, mFc Tag)	0.758	13	MERS-CoV_S1-RBD, N-(AA367-606, His Tag)	0.632
14	SARS-CoV_PLpro	0.736	14	SARS-CoV-2_S1, (His Tag)	0.631
15	SARS-CoV-2_S1, (His Tag)	0.712	15	SARS-CoV_PLpro	0.594
16	MERS-CoV_S1-RBD, N-(AA367-606, rFc Tag)	0.709	16	SARS-CoV_S1, (His Tag)	0.577
17	MERS-CoV_S1-RBD, N-(AA383-502, rFc Tag)	0.669	17	MERS-CoV_NP	0.559
18	SARS-CoV_S1, (His Tag)	0.576	18	SARS-CoV_S1-RBD, (His Tag)	0.535
19	SARS-CoV_S1-RBD, (His Tag)	0.536	19	MERS-CoV_S1-RBD, N-(AA383-502, mFc Tag)	0.533

Table 2. Receiver Operating Characteristic Area Under Curve (ROC AUC) for SARS-CoV-2, SARS-CoV, and MERS-CoV antigens. ROC AUC values for discrimination of positive and negative sera were derived for each individual antigen for both IgG and IgA and ranked, and high-performing antigens with ROC AUC $\geq$ 0.95 are indicated above the lines.

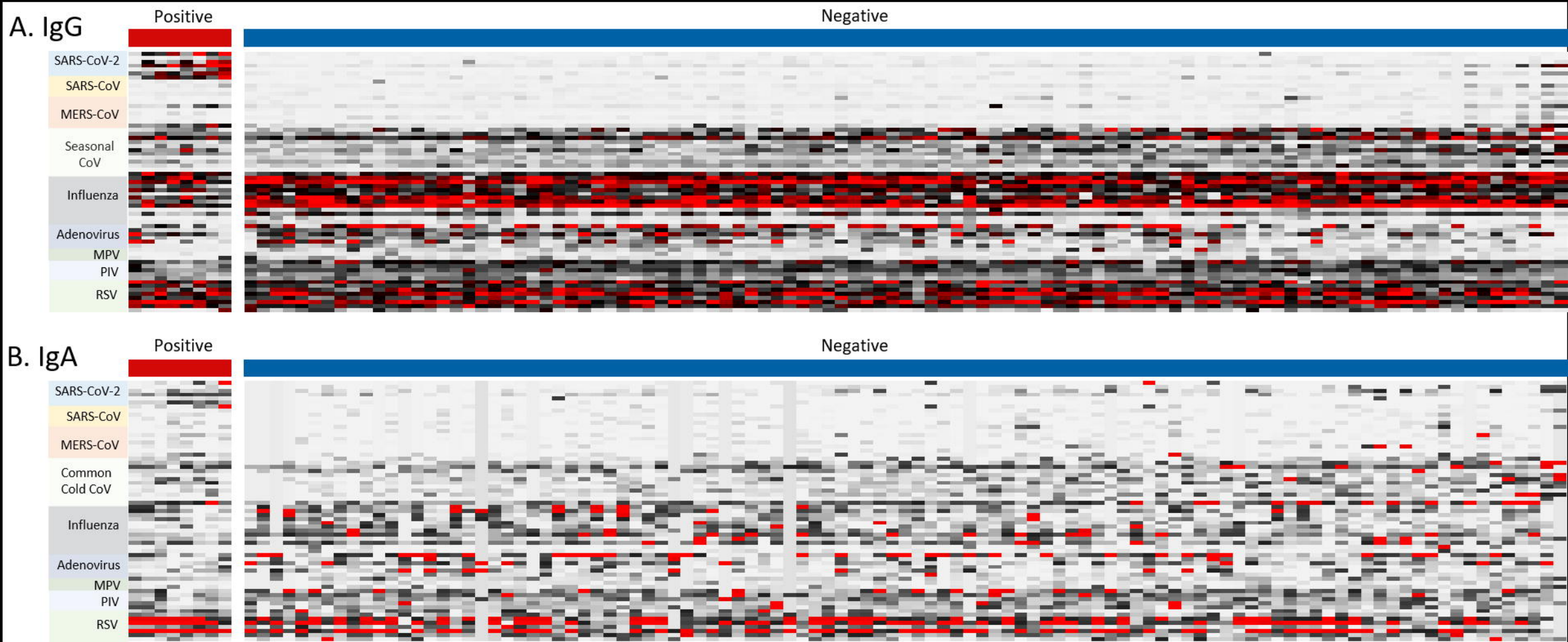
A. IgG
Positive
Negative
SARS-CoV-2
SARS-CoV
MERS-CoV
Seasonal CoV
Influenza
Adenovirus
MPV
PIV
RSV
B. IgA
Positive
Negative
SARS-CoV-2
SARS-CoV
MERS-CoV
Common Cold CoV
Influenza
Adenovirus
MPV
PIV
RSV

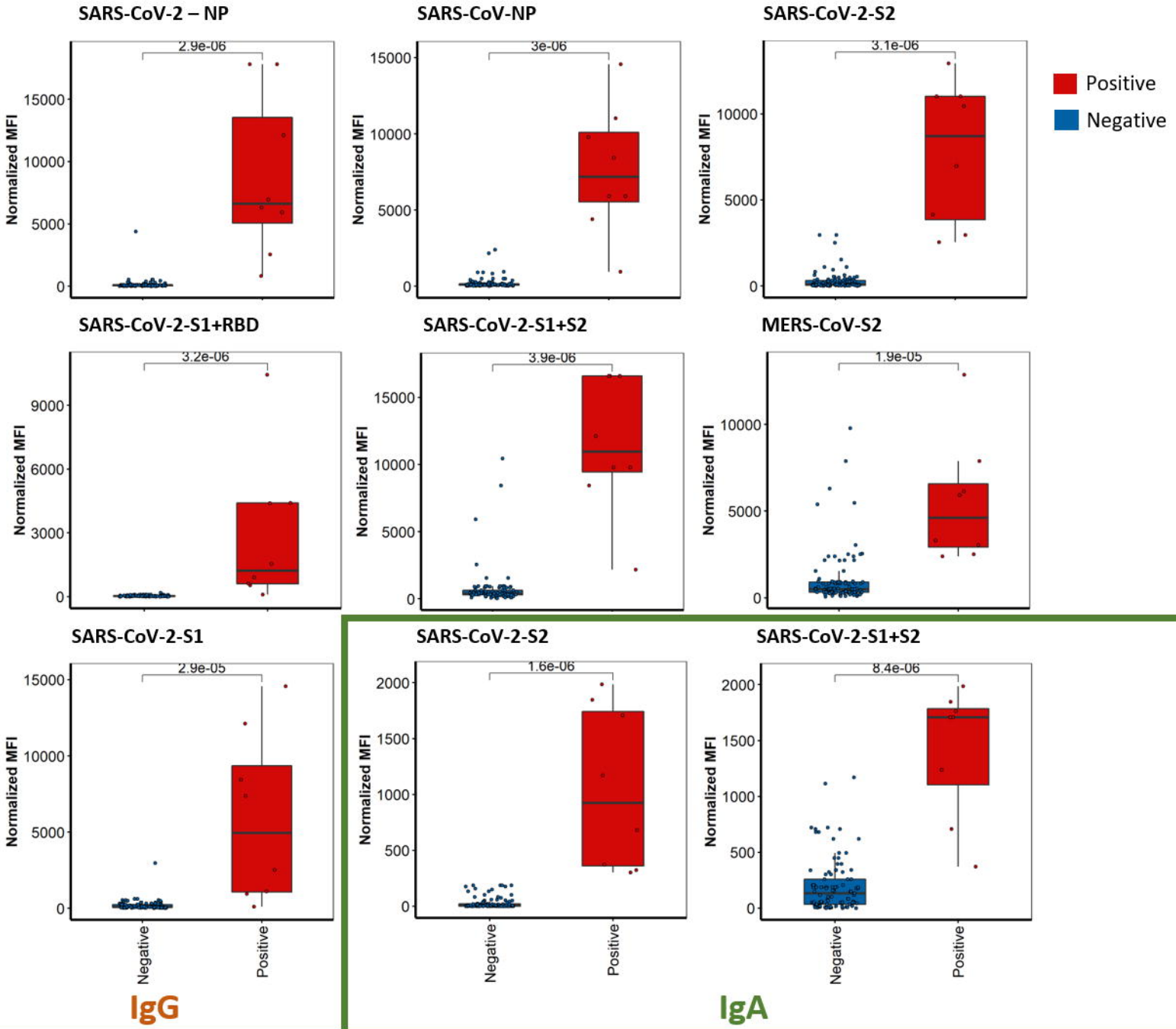
SARS-CoV-2 – NP
2.9e-06
SARS-CoV-NP
3e-06
SARS-CoV-2-S2
3.1e-06
Positive
Negative
SARS-CoV-2-S1+RBD
3.2e-06
SARS-CoV-2-S1+S2
3.9e-06
MERS-CoV-S2
1.9e-05
SARS-CoV-2-S1
2.9e-05
SARS-CoV-2-S2
1.6e-06
SARS-CoV-2-S1+S2
8.4e-06
Normalized MFI
Negative
Positive
IgG
IgA

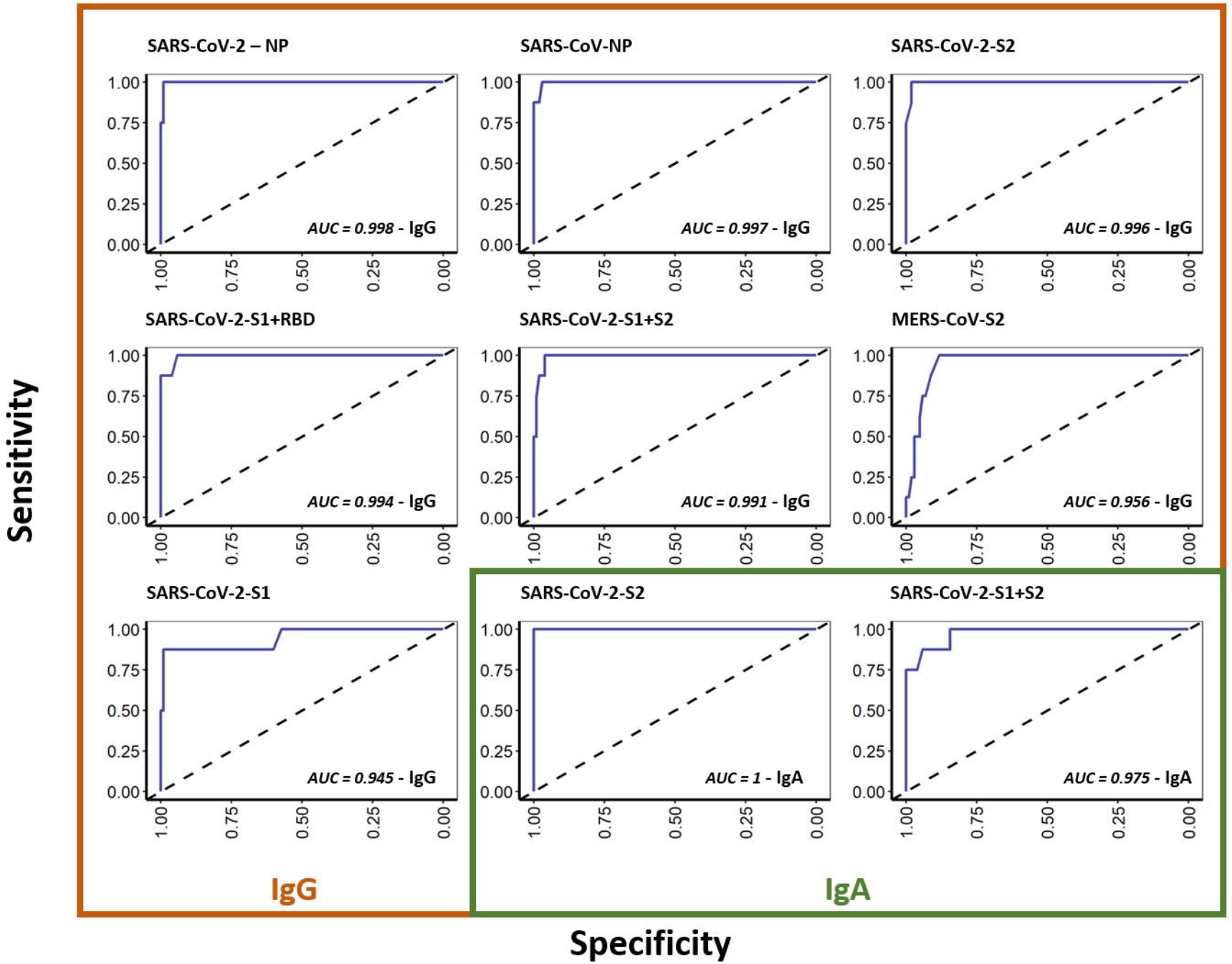
SARS-CoV-2 – NP
AUC = 0.998 - IgG
SARS-CoV-NP
AUC = 0.997 - IgG
SARS-CoV-2-S2
AUC = 0.996 - IgG
SARS-CoV-2-S1+RBD
AUC = 0.994 - IgG
SARS-CoV-2-S1+S2
AUC = 0.991 - IgG
MERS-CoV-S2
AUC = 0.956 - IgG
SARS-CoV-2-S1
AUC = 0.945 - IgG
SARS-CoV-2-S2
AUC = 1 - IgA
SARS-CoV-2-S1+S2
AUC = 0.975 - IgA
1.00
0.75
0.50
0.25
0.00
IgG
IgA
Sensitivity
Specificity

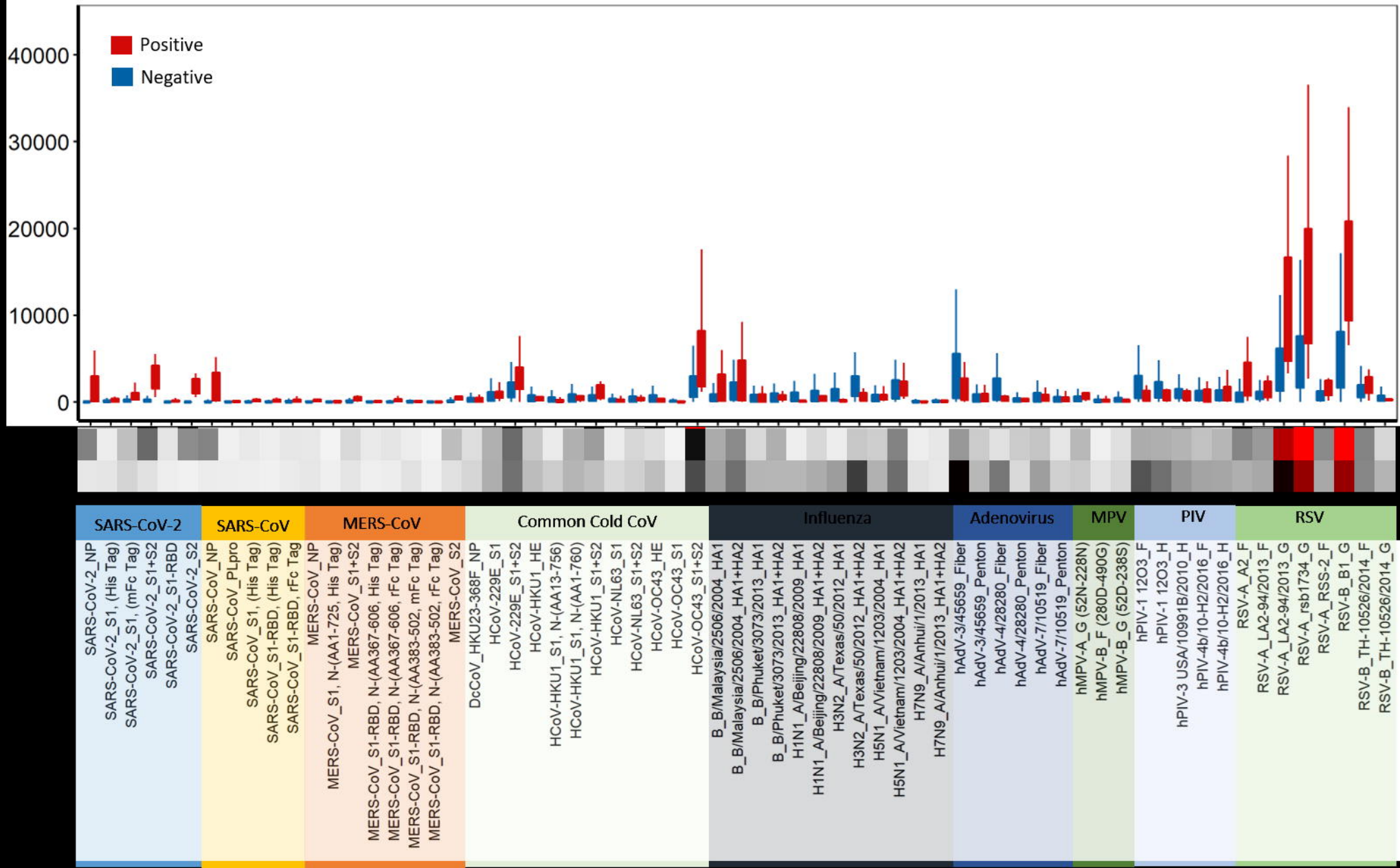
Positive
Negative
40000
30000
20000
10000
0
SARS-CoV-2
SARS-CoV
MERS-CoV
Common Cold CoV
Influenza
Adenovirus
MPV
PIV
RSV
SARS-CoV-2_NP
SARS-CoV-2_S1, (His Tag)
SARS-CoV-2_S1, (mFc Tag)
SARS-CoV-2_S1+S2
SARS-CoV-2_S1-RBD
SARS-CoV-2_S2
SARS-CoV_NP
SARS-CoV_PLpro
SARS-CoV_S1, (His Tag)
SARS-CoV_S1-RBD, (His Tag)
SARS-CoV_S1-RBD, rFc Tag
MERS-CoV_NP
MERS-CoV_S1, N-(AA1-725, His Tag)
MERS-CoV_S1+S2
MERS-CoV_S1-RBD, N-(AA367-606, His Tag)
MERS-CoV_S1-RBD, N-(AA367-606, rFc Tag)
MERS-CoV_S1-RBD, N-(AA383-502, mFc Tag)
MERS-CoV_S1-RBD, N-(AA383-502, rFc Tag)
MERS-CoV_S2
DcCoV_HKU23-368F_NP
HCoV-229E_S1
HCoV-229E_S1+S2
HCoV-HKU1_HE
HCoV-HKU1_S1, N-(AA13-756)
HCoV-HKU1_S1, N-(AA1-760)
HCoV-HKU1_S1+S2
HCoV-NL63_S1
HCoV-NL63_S1+S2
HCoV-OC43_HE
HCoV-OC43_S1
HCoV-OC43_S1+S2
B_B/Malaysia/2506/2004_HA1
B_B/Malaysia/2506/2004_HA1+HA2
B_B/Phuket/3073/2013_HA1
B_B/Phuket/3073/2013_HA1+HA2
H1N1_A/Beijing/22808/2009_HA1
H1N1_A/Beijing/22808/2009_HA1+HA2
H3N2_A/Texas/50/2012_HA1
H3N2_A/Texas/50/2012_HA1+HA2
H5N1_A/Vietnam/1203/2004_HA1
H5N1_A/Vietnam/1203/2004_HA1+HA2
H7N9_A/Anhui/1/2013_HA1
H7N9_A/Anhui/1/2013_HA1+HA2
hAdV-3/45659_Fiber
hAdV-3/45659_Penton
hAdV-4/28280_Fiber
hAdV-4/28280_Penton
hAdV-7/10519_Fiber
hAdV-7/10519_Penton
hMPV-A_G (52N-228N)
hMPV-B_F (280D-490G)
hMPV-B_G (52D-238S)
hPIV-1 12O3_F
hPIV-1 12O3_H
hPIV-3 USA/10991B/2010_H
hPIV-4b/10-H2/2016_F
hPIV-4b/10-H2/2016_H
RSV-A_A2_F
RSV-A_LA2-94/2013_F
RSV-A_LA2-94/2013_G
RSV-A_rsb1734_G
RSV-A_RSS-2_F
RSV-B_B1_G
RSV-B_TH-10526/2014_F
RSV-B_TH-10526/2014_G

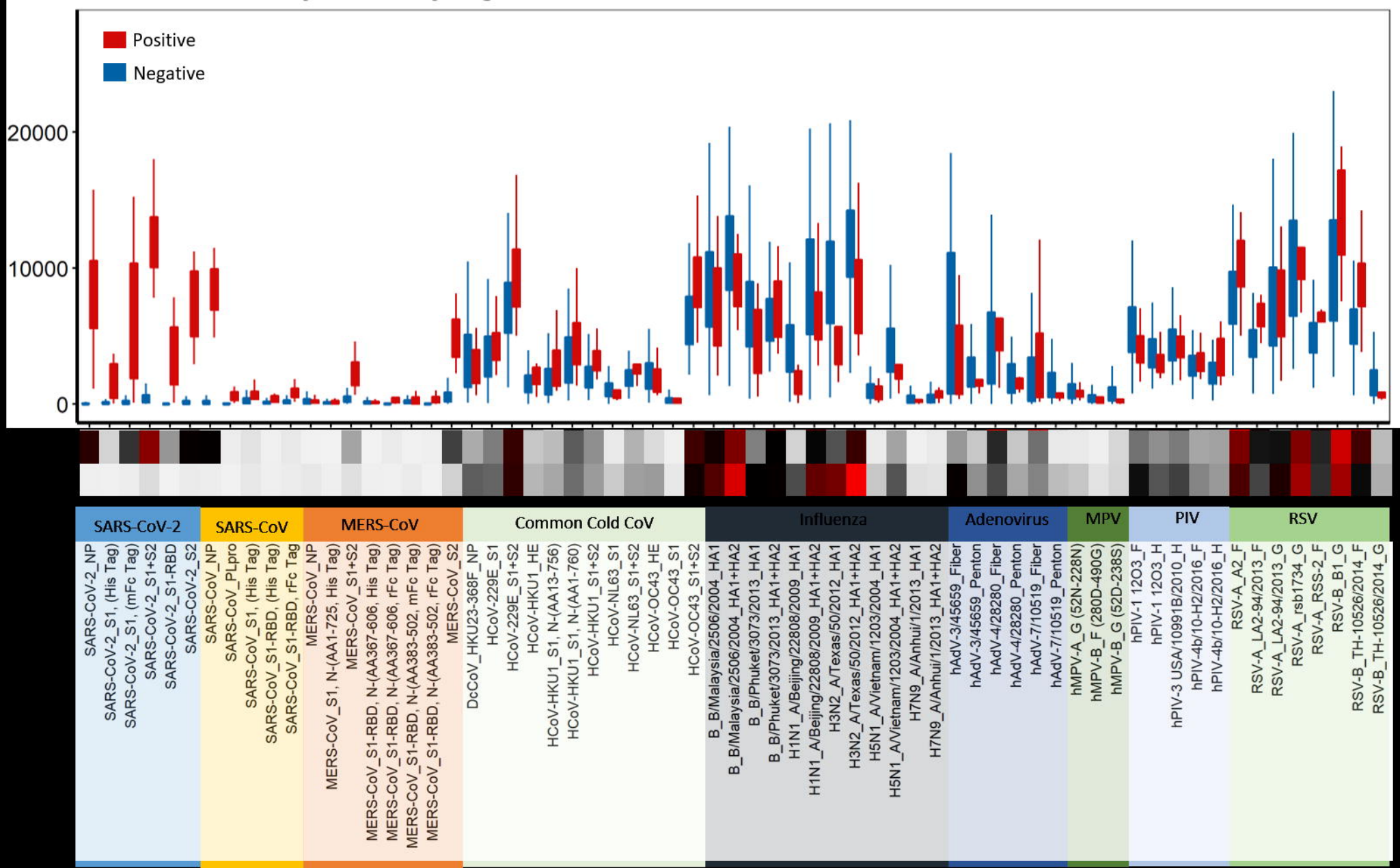
Positive
Negative
20000
10000
0
SARS-CoV-2
SARS-CoV
MERS-CoV
Common Cold CoV
Influenza
Adenovirus
MPV
PIV
RSV
SARS-CoV-2_NP
SARS-CoV-2_S1, (His Tag)
SARS-CoV-2_S1, (mFc Tag)
SARS-CoV-2_S1+S2
SARS-CoV-2_S1-RBD
SARS-CoV-2_S2
SARS-CoV_NP
SARS-CoV_PLpro
SARS-CoV_S1, (His Tag)
SARS-CoV_S1-RBD, (His Tag)
SARS-CoV_S1-RBD, rFc Tag
MERS-CoV_NP
MERS-CoV_S1, N-(AA1-725, His Tag)
MERS-CoV_S1+S2
MERS-CoV_S1-RBD, N-(AA367-606, His Tag)
MERS-CoV_S1-RBD, N-(AA367-606, rFc Tag)
MERS-CoV_S1-RBD, N-(AA383-502, mFc Tag)
MERS-CoV_S1-RBD, N-(AA383-502, rFc Tag)
MERS-CoV_S2
DcCoV_HKU23-368F_NP
HCoV-229E_S1
HCoV-229E_S1+S2
HCoV-HKU1_HE
HCoV-HKU1_S1, N-(AA13-756)
HCoV-HKU1_S1, N-(AA1-760)
HCoV-HKU1_S1+S2
HCoV-NL63_S1
HCoV-NL63_S1+S2
HCoV-OC43_HE
HCoV-OC43_S1
HCoV-OC43_S1+S2
B_B/Malaysia/2506/2004_HA1
B_B/Malaysia/2506/2004_HA1+HA2
B_B/Phuket/3073/2013_HA1
B_B/Phuket/3073/2013_HA1+HA2
H1N1_A/Beijing/22808/2009_HA1
H1N1_A/Beijing/22808/2009_HA1+HA2
H3N2_A/Texas/50/2012_HA1
H3N2_A/Texas/50/2012_HA1+HA2
H5N1_A/Vietnam/1203/2004_HA1
H5N1_A/Vietnam/1203/2004_HA1+HA2
H7N9_A/Anhui/1/2013_HA1
H7N9_A/Anhui/1/2013_HA1+HA2
hAdV-3/45659_Fiber
hAdV-3/45659_Penton
hAdV-4/28280_Fiber
hAdV-4/28280_Penton
hAdV-7/10519_Fiber
hAdV-7/10519_Penton
hMPV-A_G (52N-228N)
hMPV-B_F (280D-490G)
hMPV-B_G (52D-238S)
hPIV-1 12O3_F
hPIV-1 12O3_H
hPIV-3 USA/10991B/2010_H
hPIV-4b/10-H2/2016_F
hPIV-4b/10-H2/2016_H
RSV-A_A2_F
RSV-A_LA2-94/2013_F
RSV-A_LA2-94/2013_G
RSV-A_rsb1734_G
RSV-A_RSS-2_F
RSV-B_B1_G
RSV-B_TH-10526/2014_F
RSV-B_TH-10526/2014_G